Viscoelastic Fluid Simulation based on the Combination of Viscous and Elastic Stresses

Nobuhiko Mukai[1,2,3], Ren Morooka[1], Takuya Natsume[2] and Youngha Chang[1,2]
[1]*Computer Science, Tokyo City University, 1-28-1 Tamazutsumi, Setagaya, Tokyo, Japan*
[2]*Graduate School of Integrative Science and Engineering, Tokyo City University, 1-28-1 Tamazutsumi, Setagaya, Tokyo, Japan*
[3]*Institute of Industrial Science, the University of Tokyo, 4-6-1, Komaba, Meguro, Tokyo, Japan*

Keywords: Particle Method, Viscoelastic Fluid, Spinnability, Cauchy's Equation of Motion, Constitutive Equation.

Abstract: It is one of the challenging issues to simulate and visualize liquid behavior, especially the behavior of the viscoelastic fluid because it has both characteristics of viscosity and elasticity. Although Newtonian fluid, which sharing stress is proportional to the velocity gradient, is often analyzed with the ordinal governing equations that are Navier-Stokes equation and the equation of continuity, viscoelastic fluid behavior is so complex that there are no established governing equations, especially for the constitutive equation. Then, some studies used the Finite Element Method, and others developed a point-based method. In addition, the viscoelastic fluid has a unique characteristic called "Spinnability". The fluid is stretched so long like a string and shrinks very fast when it is ruptured. Therefore, we have been performing viscoelastic fluid simulations based on Cauchy's equation of motion by devising the stress term in the constitutive equation. In this paper, we report a viscoelastic fluid simulation based on the combination of viscous and elastic stresses.

1 INTRODUCTION

Computer graphics can visualize almost all of the things from artificial objects to natural phenomena. However, the visualization has no meaning without precise simulations. One of the most difficult and challenging issues is to simulate and visualize liquid behavior precisely, because the liquid shape changes dynamically and its boundary is very clear. In the liquid simulations, Newtonian fluid is comparatively simple since the relation between the shearing stress and the velocity gradient is linear.

However, there are many non-Newtonian fluids in the world, and one of them is called "viscoelastic fluid" that has two characteristics of viscosity and elasticity, and the relation between the shearing stress and the velocity gradient is not linear. The behavior is so complex that there are no established governing equations, especially for the constitutive equation. There are some studies that use FEM (Finite Element Method) or SM (Spring Mass) model, and others employ several kinds of methods such as a point-based method. In addition, the viscoelastic fluid has a unique characteristic called "spinnability". The fluid can be stretched so long as if it is a string, and then it shrinks very fast when it is ruptured. There is no previous work that can represent the behavior of spinnability.

Then, we have been trying to simulate and visualize the behavior of spinnability based on Cauchy's equation of motion. In the equation, there is a term of "deviatoric stress", which should be composed of viscous and elastic stresses, because the viscoelastic fluid has two characteristics of viscosity and elasticity. In our previous works, we treated the deviatoric stress as a linear combination of viscous and elastic stresses, where the sum of the coefficients for viscosity and elasticity equals to 1.0.

On the other hand, the behavior of the viscoelastic fluid suddenly changes at the rupture point when it begins to be ruptured. Therefore, in this paper, we decide the coefficients of the linear combination of viscous and elastic stresses experimentally, and show the comparison of the simulation results for several kinds of parameters with real viscoelastic fluid behavior.

Mukai, N., Morooka, R., Natsume, T. and Chang, Y.
Viscoelastic Fluid Simulation based on the Combination of Viscous and Elastic Stresses.
DOI: 10.5220/0010615901720178
In *Proceedings of the 11th International Conference on Simulation and Modeling Methodologies, Technologies and Applications (SIMULTECH 2021)*, pages 172-178
ISBN: 978-989-758-528-9

2 RELATED WORKS

Related to Newtonian fluid works, there is a survey that shows two types of studies: hydrodynamic theory based research and experimental based works (Mould and Yang, 1997), and also there is another investigation published during the 1980s and 1990s (Iglesias, 2004). In addition, there is a survey on computer graphics based ocean simulations and the rendering (Darles et al., 2011), which shows two types of methods: physics based methods using Navier-Stokes equation and empirical law based oceanographic methods.

Some people employed a mesh modeling to represent ocean waves (Hinsinger et al., 2002), irregular long crest waves (Cui et al., 2004), and vast ocean scene (Dupuy and Bruneton, 2012), because ocean waves have continuous smooth surfaces. The drawback of the mesh modeling is re-meshing that takes a lot of time and is necessary when the topology changes. Then, others utilized a particle method. SPH (Smoothed Particle Hydrodynamics) is one of the particle methods, and they presented water pouring into a glass (Müller et al., 2003) and river flowing (Kipfer and Westermann, 2006).

As for the fluid behavior simulations, there are two kinds of methods: Eulerian (grid based) and Lagrangian (particle based) methods. There are some studies that utilized Eulerian method to propose an optimized grid for GPU (Graphics Processing Unit) (Chentanez and Müller, 2010a) and to represent freezing ice with air bubbles (Nishino et al., 2012). On the other hand, there are other studies that employed semi-Lagrangian method to represent viscous liquids interacting with 3D objects (Foster and Fedkiw, 2001) and to represent bubbles with Voronoi diagram (Busaryev et al., 2012).

Moreover, other people used a hybrid method of Eulerian and Lagrangian to represent bubbles in water (Hong et al., 2008) and spray or splash (Chentanez and Müller, 2010b). There is also a method to animate viscous fluid with collision between particles and obstacles (Miller, 1989), and a parallel particle rendering system that allows to treat particles with different shapes, sizes, colors and transparencies (Sims, 1990). In addition, some studies proposed particle level-set algorithms to visualize many kinds of bubble shapes (Greenwood and House, 2004) and fine splash particles (Geiger et al., 2006). There are also some works that employed a level set method to present bubbles in liquid and gas interaction (Kim et al., 2007), and that also used a particle level set method for dense liquid volume and utilized a particle method for the diffused regions (Losasso et al., 2008).

For the simulations of the viscoelastic fluid, some people used a spring-mass system to visualize an egg dropping on the floor (Tamura et al., 2005), and others employed Finite Element methods to represent large plastic deformation of solid materials and to simulate the complex elastic and plastic behavior of viscoelastic materials (Bargtei et al., 2007) (Wojtan and Turk, 2008). These utilized Eulerian method.

On the other hand, there is a study that employed a particle based method for a viscoelastic fluid simulation (Clavet et al., 2005); however, the method also added springs to accomplish elastic and nonlinear plastic effects. The other research proposed a new method called “Material Point Method” to simulate foams and sponges, and employed Oldroyd-B model to preserve the plastic volume (Ram et al., 2015). There is also another method that developed a constrained dynamics solver by extending a position based dynamics method to represent whipped cream and strawberry syrup (Barreiro et al., 2017). These methods are particle methods or hybrid methods, and these studies do not obey Navier-Stokes equation as the governing equation, although some works employ the conservation of mass and momentum.

In addition, there is a research that used a grid based method with level set to animate viscoelastic fluids such as mucus, liquid soap, and so on (Goktekin et al., 2004). On the other hand, there is another work that utilized SPH based method to visualize melting and flowing of the viscoelastic fluid (Chang et al., 2009). Although these studies used different methods, they both employed Navier-Stokes equation as the governing equation, because the viscoleastic fluid has the characteristics of liquid and Navier-Stokes equation is the established governing equation to analyze fluid behavior. In addition, they added viscosity and elasticity terms to Navier-Stokes equation as the external term.

Navier-stokes equation is the established governing equation of fluid, and the viscoelastic fluid has two characteristics of viscosity and elasticity. Viscosity is a feature of fluid, while elasticity is another feature of elastic body that is a kind of continuum. Then, the governing equation of the viscoelastic fluid should be Cauchy’s equation of motion, which is the fundamental equation of Navier-Stokes equation including “deviatoric stress” that has both viscous and elastic stresses.

Therefore, we have been trying to simulate the behavior of the viscoelastic fluid by introducing a linear combination of viscosity and elasticity for deviatoric stress term of Cauchy’s equation of motion, and to evaluate the stretched length of the viscoelastic fluid to visualize spinnability (Mukai et al., 2010) (Mukai

et al., 2018) (Mukai et al., 2019). In the previous work, the sum of the coefficients of the linear combination of viscosity and elasticity was 1.0, since the deviatoric stress is composed of viscous and elastic stresses.

However, the behavior of the viscoelastic fluid changes dynamically between before and after the rupture. When the fluid is ruptured after being stretched, it shrinks very fast. In the behavior of the viscoelastic fluid, the effect of viscosity is larger than that of elasticity all the time; however the effect of elasticity becomes a little bit larger after it is ruptured because the fluid shrinks very fast and the characteristics of elasticity appear. Then, in this simulation, the coefficients of the linear combination of viscosity and elasticity are decided experimentally, and we show the simulation results with the different coefficients and the comparison of them with real viscoelastic fluid behavior.

3 METHOD

We employ MPS (Moving Particle Semi-implicit) method for the simulation, which is one of particle methods and was developed by Koshizuka and Oka for incompressible fluid analysis (Koshizuka and Oka, 1996). In this research, the governing equations are the equation of continuity (Eq.(1)) and Cauchy's equation of motion (Eq.(2)), which are described in the following.

Equation of continuity:

$$\frac{d\rho}{dt} = 0 \tag{1}$$

Cauchy's equation of motion with surface tension:

$$\rho\frac{d\boldsymbol{v}}{dt} = \nabla\cdot\boldsymbol{\sigma} + \boldsymbol{g} + \boldsymbol{f} = (-\nabla p\boldsymbol{I} + \nabla\cdot\boldsymbol{\tau}) + \boldsymbol{g} + \boldsymbol{f} \tag{2}$$

where, ρ is the density, t is time, $\boldsymbol{v}$ is the velocity, $\boldsymbol{\sigma}$ is the stress tensor, $\boldsymbol{g}$ is the gravity, $\boldsymbol{f}$ is the external force, p is the pressure, $\boldsymbol{I}$ is the unit matrix, and $\boldsymbol{\tau}$ is the deviatoric stress.

The target is the viscoelastic fluid that has two characteristics of viscosity and elasticity. Then, $\boldsymbol{\tau}$ should have two characteristics of viscosity and elasticity and can be written as follows (Eqs.(3)-(8)).

$$\boldsymbol{\tau} = \alpha\boldsymbol{\tau}_v + \beta\boldsymbol{\tau}_e \tag{3}$$

$$\boldsymbol{\tau}_v = 2\eta_0\boldsymbol{D} \tag{4}$$

$$\boldsymbol{D} = \frac{1}{2}(\boldsymbol{L}+\boldsymbol{L}^t), \qquad \boldsymbol{L} = \nabla\boldsymbol{V} \tag{5}$$

$$\boldsymbol{V} = (\boldsymbol{u}, \boldsymbol{v}, \boldsymbol{w}) \tag{6}$$

$$\nabla\boldsymbol{V} = \begin{bmatrix} \frac{\partial \boldsymbol{u}}{\partial x} & \frac{\partial \boldsymbol{u}}{\partial y} & \frac{\partial \boldsymbol{u}}{\partial z} \\ \frac{\partial \boldsymbol{v}}{\partial x} & \frac{\partial \boldsymbol{v}}{\partial y} & \frac{\partial \boldsymbol{v}}{\partial z} \\ \frac{\partial \boldsymbol{w}}{\partial x} & \frac{\partial \boldsymbol{w}}{\partial y} & \frac{\partial \boldsymbol{w}}{\partial z} \end{bmatrix} \tag{7}$$

$$\boldsymbol{\tau}_e = 2\mu\boldsymbol{\varepsilon}, \qquad \mu = \frac{E}{2(1+\nu)} \tag{8}$$

where, $\boldsymbol{\tau}_v$ and $\boldsymbol{\tau}_e$ are viscous and elastic terms of deviatoric stress, respectively, and α and β are the linear combination coefficients. η_0 is zero shear viscosity, $\boldsymbol{V}$ is the particle velocity, $\boldsymbol{\varepsilon}$ is the distortion tensor, E is Young's modulus and ν is Poisson's ratio.

In our previous study (Mukai et al., 2019), $\alpha+\beta = 1$ because viscoelastic stress is composed of viscous and elastic stresses. However, the behavior of viscosity and elasticity is different, and the effect of viscosity is dominant all the time, while the effect of elasticity becomes a little bit larger after the fluid is ruptured since it shrinks very fast like a rubber, which shows the characteristics of elasticity and is called "spinnability". Then, in this research, we decide the parameters of α and β experimentally. The value of α is larger than that of β all the time, because the effect of viscosity is dominant. On the other hand, the value of β depends on the density of the narrowest part of the fluid, because the fluid shrinks very fast at the middle part of it. Then, β can be calculated with the following equation (Eq.(9)).

$$\beta = \left(1 - \frac{n^k}{n^0}\right) C \tag{9}$$

where, n^0 is the initial particle number density, n^k is the particle number density of the narrowest part at the time k, and C is the dominant coefficient for elasticity, which is decided experimentally.

4 HIGH PRECISION CALCULATION

The original MPS method developed by Koshizuka and Oka (Koshizuka and Oka, 1996) assumes that the particles are regularly arranged. Then, the calculation becomes unstable when the particle arrangement is imbalanced. In this study, we adopt some high order MPS methods to stabilize the calculation even when the particle arrangement is imbalanced. One of the stabilization is for the Poisson equation of pressure

calculation. We use the model with the velocity divergence term, which was proposed by Tanaka and Masunag (Tanaka and Masunaga, 2010).

The original Laplacian of pressure developed by Kishizuka and Oka (Koshizuka and Oka, 1996) was as folllows (Eq.(10)).

$$< \nabla^2 P >_i^{k+1} = \frac{\rho}{\Delta t^2} \frac{n^0 - n_i^k}{n^0} \tag{10}$$

where, $< \nabla^2 P >_i^{k+1}$ is the Laplacian of the pressure for a particle i at the time step $k+1$, Δt is the time step, n_i^k is the particle number density of a particle i at the time step k. On the other hand, the Laplacian of pressure is calculated as follows (Eq.(11)) by the method proposed by Tanaka and Masunaga (Tanaka and Masunaga, 2010).

$$< \nabla^2 P >_i^{k+1} = \frac{\rho}{\Delta t} \nabla \cdot \boldsymbol{u}_i^* + \gamma \frac{\rho}{\Delta t^2} \frac{n^0 - n_i^k}{n^0} \tag{11}$$

where, $\boldsymbol{u}_i^*$ is the provisional velocity vector of the particle i, and γ is the relaxation coefficient, which is set depending on the problem. In this simulation, it is set as 0.2 according to the pre-calculation result. For an ideal incompressible fluid, $\nabla \cdot \boldsymbol{u}$ equals to 0; however, in computer simulations, it does not equal to 0. Then, Eq.(11) considers the term for the precise pressure calculation.

The other stabilization is for the calculation of the pressure gradient. For this purpose, we employ a high order gradient model developed by Iribe and Nakaza (Iribe and Nakaza, 2011). Moreover, in order to prevent the excessive approach of particles, the model developed by Monaghan (Monaghan, 2000) is used, which considers the artificial repulsive force that is added to the gradient model developed by Iribe and Nakaza (Iribe and Nakaza, 2011). The original gradient of the pressure developed by Koshizuka and Oka (Koshizuka and Oka, 1996) was as follows (Eq.(12)).

$$< \nabla P >_i = \frac{d}{n^0} \sum_{j \neq i} \frac{P_j - \hat{P}_i}{|\boldsymbol{r}_j - \boldsymbol{r}_i|^2} (\boldsymbol{r}_j - \boldsymbol{r}_i) \omega(|\boldsymbol{r}_j - \boldsymbol{r}_i|) \tag{12}$$

On the other hand, the high order pressure gradient is calculated with the method developed by Monaghan (Monaghan, 2000) in the following (Eq.(13)).

$$< \nabla P >_i = \left[\frac{1}{n^0} \sum_{j \neq i} \frac{(\boldsymbol{r}_j - \boldsymbol{r}_i)}{|\boldsymbol{r}_j - \boldsymbol{r}_i|} \otimes \frac{(\boldsymbol{r}_j - \boldsymbol{r}_i)}{|\boldsymbol{r}_j - \boldsymbol{r}_i|} \omega(|\boldsymbol{r}_j - \boldsymbol{r}_i|) \right]^{-1} \left[\frac{1}{n^0} \sum_{j \neq i} \frac{P_j - \hat{P}_i}{|\boldsymbol{r}_j - \boldsymbol{r}_i|^2} (\boldsymbol{r}_j - \boldsymbol{r}_i) \omega(|\boldsymbol{r}_j - \boldsymbol{r}_i|) \right] \tag{13}$$

where, $\otimes$ is the tensor product, and $\hat{P}_i$ is the minimum pressure in the radius of influence so that $\hat{P}_i$ is always lower than P_j. Since $P_j - \hat{P}_i$ is always positive, the repulsive force is generated between particles i and j Then, it is possible to prevent the excessive approach of particles due to the attraction. Eq.(13) enables the calculation stable by replacing d in Eq.(12) with the inverse matrix in Eq.(13). By the calculation with Eq.(13), the pressure becomes stable even when particles are not regularly arranged, and the inverse matrix becomes a unit matrix when particles are regularly arranged. In this case, Eq.(13) is equivalent to Eq.(12).

5 SIMULATION

Table 1 and 2 show the specifications of the PC and the parameters used for the simulation, respectively.

Table 1: Specification of the PC used in the simulation.

OS	Windows 10 Education 64 bit
CPU	Intel Core i5-8400 2.8GHz
Main memory	8GB
GPU	GeForce GTX 1660 SUPER with 6GB memory

Table 2: Parameters used for the simulation.

Parameter		Value	Unit
Density	ρ	1.16×10^{-3}	g/mm^3
Young's modulus	E	1.05×10^3	Pa
Poisson's ratio	ν	0.5	
Zero shear viscosity	η_0	28	$Pa \cdot s$
Initial distance of particles (= Particle radius)	l_0	0.3	mm
Pulling velocity	$\boldsymbol{v}$	18	mm/s
Time step	$\triangle t$	0.10×10^{-3}	s

Fig.1 shows the initial state of the particles, and (a) shows the side view for all particles. In the side view, the upper squared part of the particles is a solid body that is pulled up with the pulling velocity. On the other hand, the lower larger squared part of the particles is a rigid body that does not move even if other part of the particles moves. The middle cubed part of the particles is the viscoelastic fluid that is pulled according to the upper squared part of the particles. On the other hand, Fig.1 (b) shows the top view for only the viscoelastic fluid, which has four side named S1, S2, S3 and S4, which side has three particle width. In this research, we assume that the viscoelastic fluid begins to be ruptured if the particles enter in the radius of influence of the particle

in the confrontation. For example, if the particle in S1 enters in the radius of influence of the particle in S3, the viscoelastic fluid begins to be ruptured.

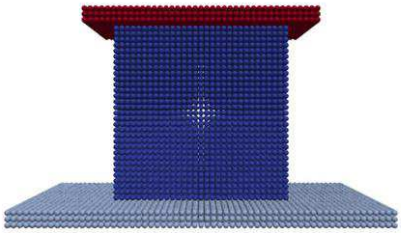

(a) Side view

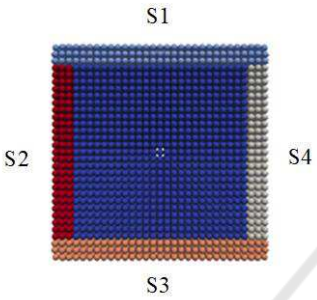

(b) Top view

Figure 1: Initial state of particles.

Table 3 shows the specification of the particles shown in Fig.1.

Table 3: Particle specification.

Part	Size [mm] (Width×Depth×Hight)	# of particles
Upper	12.3×12.3×0.9	5,043
Middle	9.3× 9.3×9.3	29,791
Lower	18.9×18.9×0.9	11,907

6 RESULTS

In the simulation, we used 0.97 and 0.95 as α for before and after the rupture of the stretched viscoelastic fluid, respectively. The value of α is large because we have found experimentally that the effect of viscosity is larger than that of elasticity all the time. In addition, if α is larger than 0.97, viscoelastic fluid behaves as if it is Newtonian fluid, and it flows down on the floor. It does not show the characteristic of elasticity if α is larger than 0.97. In addition, the effect of elasticity becomes a little bit larger after the rupture, because the characteristics of elasticity appear and the fluid shrinks very fast like a rubber. This means that the characteristics of viscosity become a little bit lower compared with that in the before. Then, the value of α after the rupture is lower than that before the rupture.

On the other hand, β is decided with Eq.(9), and the maximum value is C when the particle number density n^k is 0, which means that stretched viscoelastic fluid is completely ruptured. Then, we set 0.03, 0.05 and 0.07 as C. One reason is that 0.03+0.97=1, which means that 0.03 is the complement of 0.97 that is the value of α before the rupture. The second reason is that 0.05+0.95=1, which means that 0.05 is the complement of 0.95 that is the value of α after the rupture. Setting 0.07 as C is the confirmation that the effect of viscosity is too strong for the viscoelastic fluid to be stretched, because 0.07+0.95=1.02>1.0.

Fig.2 shows the three kinds of simulation images after 750 steps and a real viscoelastic fluid named "guar gum".

In Fig.2 (a), (b), and (c), the middle part width becomes thinner as C becomes larger, because larger C means the less effectiveness of viscosity and the more effectiveness of elasticity. All the stretched lengths of three images are shorter than a real viscoelastic fluid shown in Fig.2 (d). Spinnability, which is a unique characteristic of viscoelastic fluid, has three features: 1) it can be stretched very long, 2) the middle part of it becomes very thin, and 3) it shrinks very fast when it is ruptured. In the simulation results, it seems that the feature 2) is satisfied; however, the feature 1) is not satisfied. All three stretched lengths are shorter than the real viscoelastic fluid shown in (d). In fact, the stretched length in the simulation using $C = 0.05$ was 1.4[mm], while the real viscoelastic fluid stretched length was 41.8[mm] that was measured in the movie. In the feature 3), the shrinking time in the simulation using $C = 0.05$ was $500[ms]$, while it was $4,333[ms]$ in the real viscoelastic fluid, which means that the viscoelastic fluid in the simulation shrunk faster than the real fluid, although it is partly due to the shorter stretching than that of the real fluid. As a result, the effect of viscosity should be stronger than that of elasticity to realize spinnability in the viscoelastic fluid simulation. However, the too large value of α makes the viscoelastic fluid behave as if it is Newtonian fluid.

7 CONCLUSIONS

In this paper, we have adopted two high order calculations of pressure to simulate the behavior of the viscoelastic fluid precisely. One is for Laplacian of

Figure 2: Simulation results and a real viscoelastic fluid.

pressure that is used in the Poisson equation, and the other is for the gradient of pressure, which prevents the excessive approach of particles. In the simulation of the viscoelastic fluid behavior, we have employed the idea of the combination for viscous and elastic stresses of deviatoric stress; however, the coefficients of the combination were decided experimentally keeping the sum of coefficients equals to almost 1.0.

As the result of the simulation, one of the features in spinnability was satisfied, and the middle part of the fluid became very thin. However, the stretched length in the simulation was shorter than that in the real fluid, and the shrinking time in the simulation was also shorter. One of the reasons is the shortage of the particles used in the simulation to realize the precise behavior of viscoelastic fluid. Although the simulation results differed from the behavior of the reawhich arel viscoelastic fluid "guar gum", we have confirmed that the combination of viscous and elastic stresses can be one solution for the analysis of viscoelastic stress. In this paper, the linear combination coefficients of α and β, and the elastic dominant coefficient of C were decided experimentally; however, these coefficients shoud be decided theoretically with some evidence.

In the future, we have to reconsider the combination way of viscous and elastic stresses in deviatoric stress term to realize the two remaining characteristics of spinnability, and we also have to use more particles to simulate viscoelastic fluid behavior precisely.

REFERENCES

Bargtei, A., Wojtan, C., Hodgins, J., and Turk, G. (2007). A finite element method for animating large viscoplastic flow. *ACM Transactions on Graphics*, 26(3):Article No.16.

Barreiro, H., García-Fermández, I., Alduán, I., and Otaduy, M. (2017). Conformation constraints for efficient viscoelastic fluid simulation. *ACM Transactions on Graphics*, 36(6):Article No.221.

Busaryev, O., Dy, T., Wang, H., and Ren, Z. (2012). Animating bubble interactions in a liquid foam. *ACM Transactions on Graphics*, 31(4):63:1–63:8.

Chang, Y., Bao, K., Liu, Y., Zhu, J., and Wu, E. (2009). A particle-based method for viscoelastic fluids animation. In *ACM Symposiumon virtual reality software and technology*, pages 463–468.

Chentanez, N. and Müller, M. (2010a). Real-time simulation of large bodies of water with small scale details. In *ACM SIGGRAPH/Eurographics symposium on computer animation*, pages 197–206.

Chentanez, N. and Müller, M. (2010b). Real-time simulation of large bodies of water with small scale details.

Clavet, S., Beaudoin, P., and Poulin, P. (2005). Particle-based viscoelastic fluid simulation. In *ACM SIGGRAPH/Eurographics Symposium on computer animation*, pages 219–228.

Cui, X., Yi-cheng, J., and Xiu-wen, L. (2004). Real-time ocean wave in multi-channel marine simulator. In *ACM SIGGRAPH international conference on virtual reality continuum and its application in industry*, pages 332–335.

Darles, E., Crespin, B., Ghazanfarpour, D., and Gonzato, J. (2011). A survey of ocean simulation and rendering

techniques in computer graphics. In *Computer Graphics Forum*, volume 30, pages 43–60.

Dupuy, J. and Bruneton, E. (2012). Real-time animation and rendering of ocean whitecaps. In *SIGGRAPH Asia, Technical Briefs*, page Article No.15.

Foster, N. and Fedkiw, R. (2001). Practical animation of liquids. In *ACM SIGGRAPH*, pages 23–30.

Geiger, W., Leo, M., Rasmussen, N., Losasso, F., and Fedkiw, R. (2006). So real it'll make you wet. In *ACM SIGGRAPH Sketches*, page Article No.20.

Goktekin, T., Bargteil, A., and O'Brien, J. (2004). A method for animating viscoelastic fluids. *ACM Transactions on Graphics*, 23(3):463–468.

Greenwood, S. and House, D. (2004). Better with bubbles: Enhancing the visual realism of simulated fluid. In *ACM SIGGRAPH/Eurographics symposium on computer animation*, pages 287–296.

Hinsinger, D., Neyret, F., and Cani, M. (2002). Interactive animation of ocean waves. In *ACM SIGGRAPH/Eurographics symposium on computer animation*, pages 116–166.

Hong, J., Lee, H., Yoon, J., and Kim, C. (2008). Bubbles alive. *ACM Transactions on Graphics*, 27(3):48:1–48:8.

Iglesias, A. (2004). Computer graphics for water modeling and rendering: A survey. *Future Generation Computer Systems*, 20(8):1355–1374.

Iribe, T. and Nakaza, E. (2011). An improvement of accuracy of the mps method with a new gradient calculation model (in japanese). *Journal of the Japan Society of Civil Engineers(B2)*, 67(1):36–48.

Kim, B., Liu, Y., Llamas, I., Jiao, X., and Rossignac, J. (2007). Simulation of bubbles in foam with the volume control method. *ACM Transactions on Graphics*, 26(3):98:1–98:10.

Kipfer, P. and Westermann, R. (2006). Realistic and interactive simulation of rivers. In *Graphics Interface*, pages 41–48.

Koshizuka, S. and Oka, Y. (1996). Moving-particle semi-implicit method for fragmentation of incompressible fluid. *Nuclear Science and Engineering*, 123:421–434.

Losasso, F., Talton, J., Kwatra, N., and Fedkiw, R. (2008). Two-way coupled sph and particle level set fluid simulation. *IEEE Transsactions on Visualization and Computer Graphics*, 14(4):797–804.

Miller, G. (1989). Globular dynamics: A connected particle system for animating viscous fluids. *Computers & Graphics*, 13(3):305–309.

Monaghan, J. (2000). SPH without a tensile instability. *Journal of Computational Physics*, 159(2):290–311.

Mould, D. and Yang, Y. (1997). Modeling water for computer graphics. *Computers & Graphics*, 21(6):801–814.

Müller, M., Charypsr, D., and Gross, M. (2003). Particle-based fluid simulation for interactive applications. In *ACM SIGGRAPH/Eurographics symposium on computer animation*, pages 154–159.

Mukai, N., Ito, K., Nakagawa, M., and Kosugi, M. (2010). Spinnability simulation of viscoelastic fluid. In *ACM SIGGRAPH Posters*, page Article No.18.

Mukai, N., Matsui, E., and Chang, Y. (2019). Investigation on viscoelastic fluid behavior by modifying deviatoric stress tensor. In *SIMULTECH*, pages 216–222.

Mukai, N., Nishikawa, T., and Chang, Y. (2018). Evaluation of stretched thread lengths in spinnability. In *ACM SIGGRAPH Posters*, page Article No.62.

Nishino, T., Iwasaki, K., Dobashi, Y., and Nishita, T. (2012). Visual simulation of freezing ice with air bubbles. In *SIGGRAPH Asia, Technical Briefs*, page Article No.1.

Ram, D., Gast, T., Jiang, C., Schroeder, C., Sromakhin, A., Teran, J., and Kavehpour, P. (2015). A material point method for viscoelastic fluids, foams and sponges. In *ACM SIGGRAPH/Eurographics symposium on computer animation*, pages 157–163.

Sims, K. (1990). Particle animation and rendering using data parallel computation. In *ACM SIGGRAPH*, volume 24, pages 405–413.

Tamura, N., Tsumura, N., Nakaguchi, T., and Miyak, Y. (2005). Spring-bead animation of viscoelastic materials. In *ACM SIGGRAPH Sketches*, page Article No.64.

Tanaka, M. and Masunaga, T. (2010). Stabilization and smoothing of pressure in mps method by quasi-compressibility. *Journal of Computational Physics*, 229(11):4279–4290.

Wojtan, C. and Turk, G. (2008). Fast viscoelastic behavior with thin features. *ACM Transactions on Graphics*, 27(3):Article No.47.